Open Access Online Journal on Astronomy and Astrophysics

Acta Astrophysica Taurica

www.astrophysicatauricum.org

Acta Astrophys. Tau. 5(2), 6–12 (2024)

Electric currents in unipolar active regions with different magnetic flux decay rates in sunspots

Yu.A. Fursyak, A.A. Plotnikov, V.I. Abramenko

Crimean Astrophysical Observatory, Nauchny 298409
e-mail: yuriy_fursyak@mail.ru

Received 14 October 2021

ABSTRACT

Using the magnetographic data of the Helioseismic and Magnetic Imager (HMI) instrument on board the Solar Dynamics Observatory (SDO), we calculated parameters of the magnetic field and electric currents for unipolar active regions (ARs) with low ($\leq 2.1 \times 10^{19}$ Mx h^{-1}; in total, 11 ARs were analyzed) and high ($\geq 7.0 \times 10^{19}$ Mx h^{-1}, 5 ARs were analyzed) magnetic flux decay rates in sunspots. We obtained the following results: 1) the stronger the local (small-scale) electric currents in the vicinity of a unipolar sunspot, the faster its decaying; 2) the distributed (global, large-scale) electric current around the rapidly decaying sunspots is practically zero. There cannot be expected a stabilizing effect on the decay of a sunspot; 3) in four cases of slowly decaying sunspots, a nonzero distributed electric current of up to 5.0×10^{12} A was detected. Perhaps such electric current can have a stabilizing effect on the decay of a sunspot.

Thus, our findings indicate that strong electric currents of small scales have a rather destructive effect on a sunspot, and the presence of large-scale currents can stabilize it. However, this mechanism seems not to be the only one and dominant in the processes of stabilization of unipolar sunspots.

Key words: Sun, unipolar active regions, magnetic fields, electric currents, magnetic flux decay rate

1 Introduction

When studying phenomena on the Sun, issues regarding the evolution (emergence, development, and dissipation) of sunspots are crucial as they represent the most pronounced manifestations of the magnetic field dynamics in the convective zone and solar atmosphere. The issue of sunspot dissipation was first formulated in Cowling (1946), and active research on this topic has been started since the 1970s and 1980s (see, for example, Sheeley, Bhatnagar, 1971; Meyer et al., 1974; Solov'ev, 1976a; Krivodubskii, 1983; Muller, Mena, 1987; Nye et al., 1988, and many others). In recent decades, with the emergence of new powerful instruments such as SDO (Pesnell et al., 2012), Hinode (Kosugi et al., 2007), NST(GST)/BBSO (Goode et al., 2003), and others, which enable monitoring of the Sun with high spatial (0.5″ and below) and temporal (no more than a few dozen minutes, often much less) resolution, the interest in studying the peculiarities of emergence and decay of the magnetic flux in sunspots has been renewed. This is evidenced by a series of reports dedicated to this issue presented at solar physics conferences. The advancement of computer technology also contributes to this interest, allowing for the creation of complex theoretical models describing the processes of sunspot stabilization/destabilization (e.g., Solov'ev, 1991; Zeleniy, Milovanov, 1993; Litvinenko, Wheatland, 2015, and others).

In a recent statistical study exploring the magnetic flux decay rate for sunspots of the AR, Plotnikov, Kutsenko (2021) detected the presence of two sequences of sunspot groups (see Fig. 1), with one forming a "tail" within the magnetic flux values of $(2.0 - 9.0) \times 10^{21}$ Mx with low (less than 2.1×10^{19} Mx h^{-1}) decay rates. It was found that a significant portion of these ARs belong to unipolar ones. The reason for such behavior of some unipolar ARs needs to be further investigated.

Researchers consider several different mechanisms of magnetic flux decay in sunspots. The majority of them associate the disruption of a sunspot with turbulent plasma motions in its vicinity (Meyer et al., 1974; Solov'ev, 1976a; Ivanov, Maksimov, 1978; Krivodubskii, 1983; Muller, Mena, 1987; Kubo et al., 2008; Litvinenko, Wheatland, 2015). Additionally, there is an approach suggesting that the sunspot magnetic field dissipation occurs due to the presence of moving magnetic features (MMFs), first mentioned in Harvey, Harvey (1973). Observational data (Martinez Pillet, 2002; Kubo, Shimizu, 2007) indicate that MMFs carry away more magnetic flux than the intrinsic flux decrease in a sunspot.

There are other mechanisms of sunspot stabilization/destabilization, such as the intrinsic oscillations of sunspots (Solov'ev, 1984; Solov'ev, Kirichek, 2014). Among the possible reasons leading to varying rates of magnetic

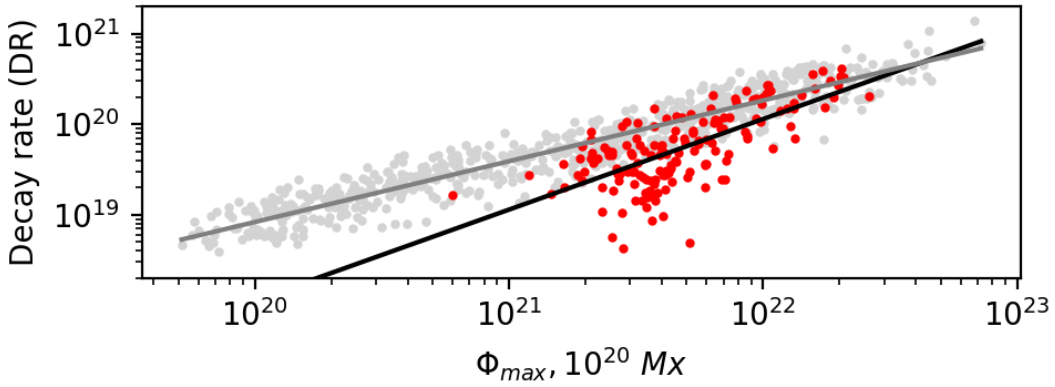

Fig. 1. Dependence of the magnetic flux decay rate in sunspots on the maximum total unsigned magnetic flux during the presence of the AR on the visible solar disk (Φ_{max}) for bipolar (gray points) and unipolar (red points) sunspot groups, as obtained in Plotnikov, Kutsenko (2021).

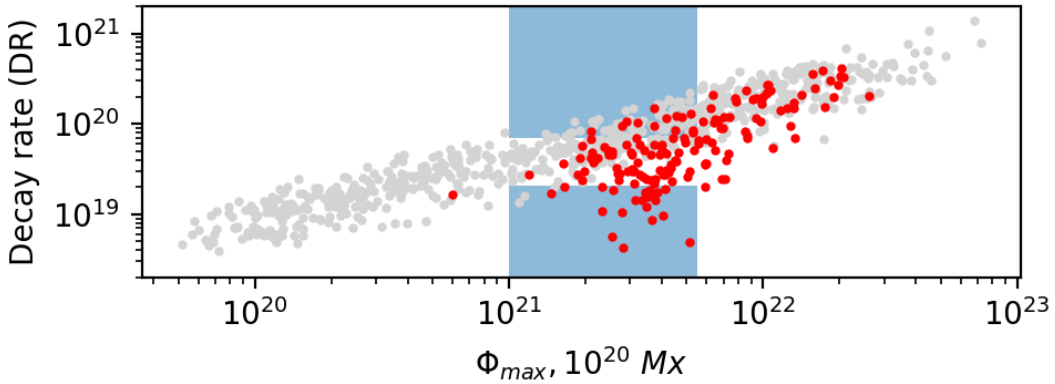

Fig. 2. Same as in Fig. 1, but indicating ranges (shaded blue areas) for the magnetic flux and magnetic flux decay rate in which a sample of unipolar ARs was selected for the study.

flux decay, researchers also distinguish a different depth of sunspot bases in the convective zone (Strecker et al., 2021).

Despite the significant interest in sunspot decay, there are very few studies considering electric currents as a factor of sunspot stabilization/destabilization (see, for example, Solov'ev, 1976b). Therefore, our objective is to investigate the sample of unipolar regions distinguished in Plotnikov, Kutsenko (2021) and determine how electric currents affect the magnetic flux decay rate in sunspots.

2 Observation Data

The main data for analysis consist of magnetograms of the magnetic field vector components at the photospheric level, obtained by the HMI/SDO instrument (Scherrer et al., 2012) with a spatial resolution of 0.5″ (≈ 363 km on the surface of the Sun) and a temporal resolution of 12 minutes.

The selection of ARs for the study was carried out according to the following conditions:

1. The AR should belong to type U or A1 at the late stage of evolution according to the magneto-morphological classification (MMC) of ARs developed at the Crimean Astrophysical Observatory (CrAO) (Zhukova, 2018; Abramenko et al., 2018); pores may be observed in the trailing part of the AR, but the main sunspot should be well developed.
2. The AR should be isolated from other ARs (i.e., only one AR should be present within one HARP (HMI/SDO Active Region Patch; Hoeksema et al., 2014).
3. The maximum total unsigned magnetic flux of the AR should be within $(1.0 - 5.5) \times 10^{21}$ Mx (see Fig. 2).
4. The magnetic flux decay rate of a sunspot should not exceed $2.1{\times}10^{19}$ Mx h^{-1} or be at least $7.0{\times}10^{19}$ Mx h^{-1} (see Fig. 2). Extreme cases were deliberately chosen to observe the expected effect.

According to the specified criteria for analysis, 11 unipolar ARs with low ($\leq 2.1 \times 10^{19}$ Mx h^{-1}) and 5 unipolar ARs with high ($\geq 7.0{\times}10^{19}$ Mx h^{-1}) magnetic flux decay rates in sunspots were selected. The main parameters of the studied ARs are presented in Table 1.

The first column of the table shows the AR number (NOAA); the second, the time of our monitoring of the corresponding AR; the third, the polarity of a sunspot in the AR. The fourth column displays the magnetic flux decay rate in a sunspot (DR; see more details in Section 3) in units of 10^{19} Mx h^{-1}. The fifth column indicates the total unsigned magnetic flux averaged over the AR monitoring time in units

Table 1. Parameters of the magnetic field and electric currents for the regions in the studied sample.

Region Number (NOAA)	AR Monitoring Time	Sunspot Polarity	DR, 10^{19} Mx h^{-1}	$\bar{\Phi}$, 10^{22} Mx	$<\|\bar{j_z}\|>$, 10^{-3} A m^{-2}	$\bar{I}_{\rm distr}$, 10^{12} A	ρ_{B_z}, %
1	**2**	**3**	**4**	**5**	**6**	**7**	**8**
11591	16.10–20.10.2012	S	0.35	0.55	2.10	4.99 ± 2.59	−91.64
12246	25.12–29.12.2014	S	0.43	0.26	1.98	−1.64 ± 1.90	−97.21
12195	26.10–30.10.2014	S	1.07	0.35	2.10	−2.17 ± 4.92	−43.62
11340	08.11–12.11.2011	N	1.46	0.25	2.09	3.46 ± 2.65	87.47
11658	17.01–20.01.2013	N	1.55	0.27	2.18	2.90 ± 3.17	72.86
11642	04.01–08.01.2013	N	1.64	0.39	2.09	0.08 ± 1.82	52.36
12061	15.05–18.05.2014	N	1.77	0.37	2.17	3.34 ± 1.78	46.47
12090	15.06–18.06.2014	S	1.85	0.38	2.26	−0.85 ± 3.75	−65.46
11423	27.02–02.03.2012	S	1.85	0.34	2.43	−0.19 ± 1.62	−64.61
11912	06.12–09.12.2013	N	1.89	0.52	2.03	2.54 ± 1.64	39.82
11537	04.08–08.08.2012	S	2.09	0.12	1.92	0.63 ± 1.63	−99.95
11695	15.03–18.03.2013	S	7.06	0.55	2.21	−0.03 ± 2.19	−63.26
12348	17.05–21.05.2015	N	7.09	0.24	2.25	0.53 ± 2.50	95.49
11757	29.05–01.06.2013	N	8.19	0.14	2.27	−0.10 ± 2.22	76.37
11649	08.01–12.01.2013	N	11.20	0.25	2.59	−1.22 ± 2.24	67.80
11621	29.11–02.12.2012	S	12.70	0.32	2.42	−1.00 ± 1.61	−78.37

of 10^{22} Mx. The parameters of the electric current (see Sections 3 and 4) – the values of the average unsigned vertical electric current density, averaged over the AR monitoring time (in units of 10^{-3} A m^{-2}), and the averaged large-scale (distributed) electric current (with error values in units of 10^{12} A) – are presented in the sixth and seventh columns, respectively. Errors in determining the distributed electric current were calculated using the least squares method. The last column of the table shows the average magnetic flux imbalance over the observation time.

To minimize errors in calculations caused by the projection effect, monitoring of each of the studied regions was carried out within a time interval during which the region was within ±35° relative to the central solar meridian (4–6 days).

3 Features of the applied methods

The value of the magnetic flux decay rate in a sunspot is calculated as the tangent of the regression line slope at the sunspot decay phase (see Fig. 3).

Vertical electric currents in the studied regions were calculated using the integral form of Ampere's law:

$$I_z = \frac{1}{\mu_0} \oint_L \boldsymbol{B}_\perp dl,$$

where μ_0 is the magnetic constant, $\boldsymbol{B}_\perp \equiv (B_x, B_y)$ is the vector of the transverse magnetic field in the photosphere, L is the closed rectangular contour, with the value of the vertical electric current I_z calculated in its central pixel. In this study, as well as in others, we used the contour L with a size of 5×5 pixels. An example of the map showing the distribution of the vertical electric current for two ARs in the analyzed sample is presented in Fig. 4. The features of the integral method for calculating the vertical electric current, as well as the reasons for choosing a contour of this particular configuration, are

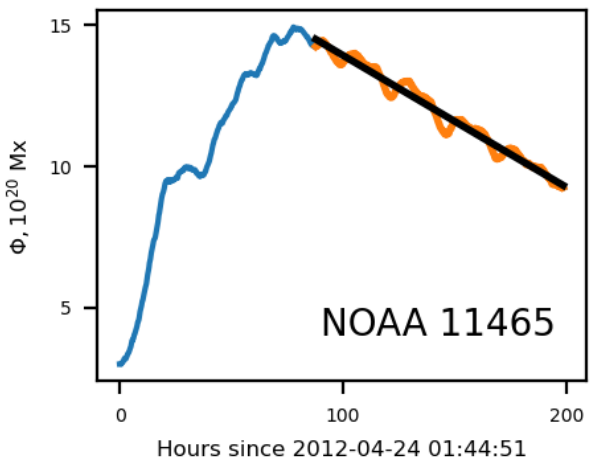

Fig. 3. Toward explanation of calculating the magnetic flux decay rate of a sunspot. The ascending (blue curve) and descending (orange curve) branches of the sunspot evolution are shown. The black line represents the linear regression during the sunspot decay phase. The tangent of this line slope angle is taken as a value of the magnetic flux decay rate.

extensively described in Fursyak (2018). The bitmap masks (indicating the boundaries of the ARs on the SHARP magnetogram, represented by the red curve) and the conf_disambig mask (blue curve in Fig. 4, highlighting pixels on the magnetogram where the 180-degree ambiguity in calculations of the azimuth of the transverse magnetic field is allowed with high confidence) are denoted by contours in the figure. The values of the electric current parameters were calculated only for pixels located within these two contours. The peripheral parts of SHARP magnetograms and corresponding maps of

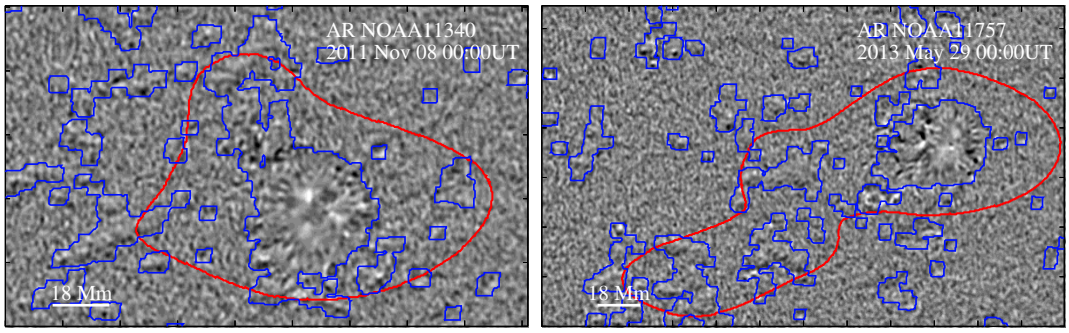

Fig. 4. Maps showing the distribution of vertical electric current density in NOAA AR 11340 (left) and 11757 (right) at the initial moment of their monitoring (see Table 1). The maps are scaled from −0.01 A m^{-2} (black) to 0.01 A m^{-2} (white). The red contour outlines the bitmap mask boundaries, while the blue contour outlines the conf_disambig mask boundaries (for more details, refer to the text).

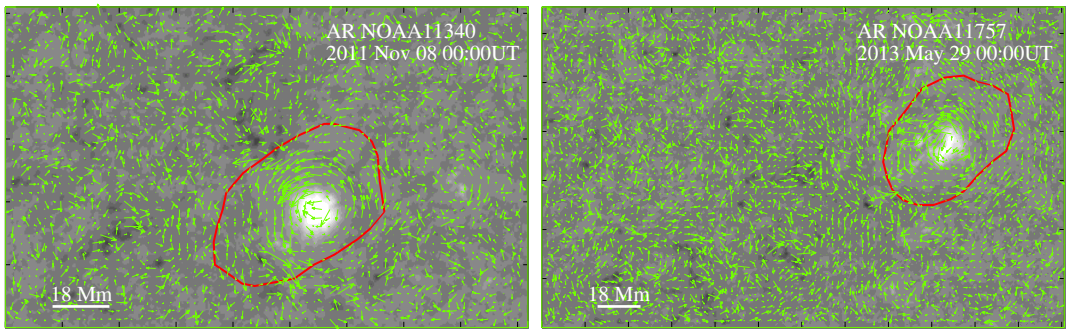

Fig. 5. Maps of the B_z component of the magnetic field (background) for NOAA AR 11340 (left) and 11757 (right) at the beginning of their monitoring, with azimuths of the vector of the nonpotential component of the observed transverse field of the AR $\boldsymbol{B}_{t\perp}$ superimposed (green arrows). The red curve indicates the contours within which the values of the distributed electric current I_{distr} were calculated based on the corresponding map of the vertical electric current density distribution.

electric current density were not taken into account, which should significantly reduce errors in calculations.

Large-scale (distributed) electric current calculations are carried out according to the method described in Fursyak et al. (2020b). The method involves identifying regular vortex structures of the nonpotential component of the transverse magnetic field ($\boldsymbol{B}_{t\perp}$) in the vicinity of large sunspots in the AR, which are caused by the presence of the significantly distributed vertical electric current. To calculate the value of the distributed electric current, an oval-shaped contour C is drawn in the vicinity of the sunspot, applying two rules: 1) inside the contour, the vector of the nonpotential component of the transverse field should have a predominant swirling direction (clockwise or counterclockwise), while outside the contour, the vector $\boldsymbol{B}_{t\perp}$ is spatially distributed chaotically; 2) the contour is drawn close to the sunspot because the vortex magnetic field induced by the current decreases inversely proportional to distance. The contour C is defined based on the first map of the $\boldsymbol{B}_{t\perp}$ distribution, and its shape remains constant throughout the monitoring time. To minimize errors in calculating the distributed electric current value due to the sunspot displacement, the contour is anchored to the center of gravity of the sunspot, which is calculated for each moment during the entire AR monitoring interval. Even a 1-pixel shift of the sunspot on the magnetogram leads to the corresponding shift of the contour by the same number of pixels. The distributed electric current value is calculated from the corresponding map of the vertical electric current distribution as the resulting electric current inside the contour C. Integrating over other contours gives us a resulting electric current value that tends toward zero. The examples of maps showing the distribution of the nonpotential component of the transverse magnetic field in two studied ARs are shown in Fig. 5. The contour C, within which the value of the distributed electric current was calculated, is shown by the red curve in Fig. 5.

4 Results

When comparing the magnetic flux decay rate in sunspots with the parameters of the electric current in unipolar ARs, the following results were obtained:

1. A statistical relation was found between the magnetic flux decay rate in a sunspot and the value of the average unsigned vertical electric current density (Fig. 6):

$$< |j_z| >= \frac{\sum |j_z|_{i,j}}{N},$$

where j_z is the vertical electric current density value in the pixel with coordinates i and j, and N is the number of pixels within the bitmap and conf_disambig masks. The

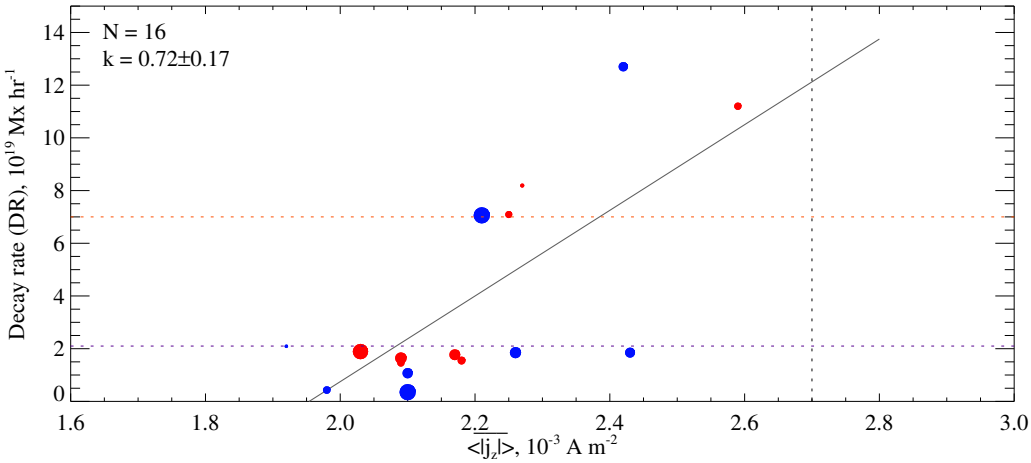

Fig. 6. Dependence of the magnetic flux decay rate in sunspots on the value of the average unsigned vertical electric current density $< |j_z| >$ for the studied sample of ARs. The boundaries of decay rates for slowly (DR$\leq 2.1 \times 10^{19}$ Mx h^{-1}) and rapidly (DR$\geq 7.0 \times 10^{19}$ Mx h^{-1}) dissipating ARs are indicated by violet and orange horizontal dashed lines, respectively. The vertical dashed line represents the boundary $< |j_z| >= 2.7 \times 10^{-3}$ A m^{-2}. Positive (N) and negative (S) polarity sunspots are marked in red and blue, respectively.

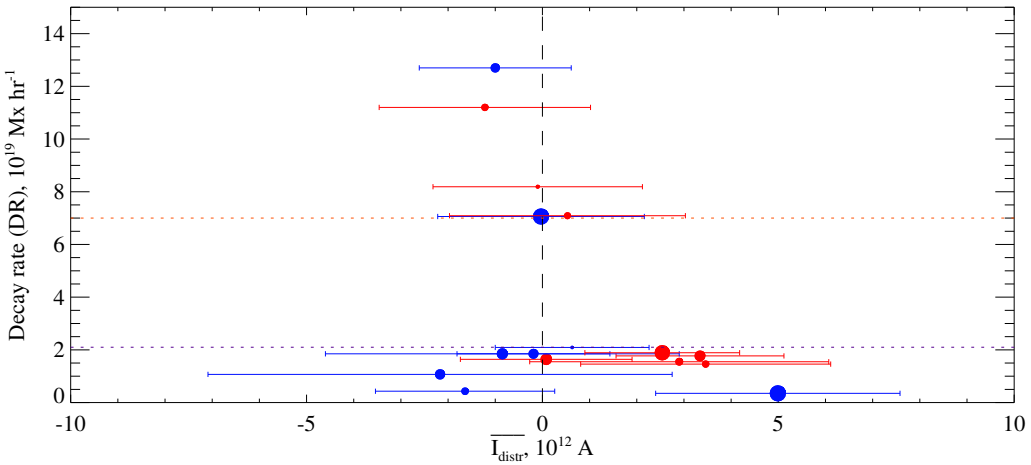

Fig. 7. Dependence of the magnetic flux decay rate in sunspots on the value of the large-scale (distributed) electric current (I_{distr}). Error bars for determining the distributed electric current values are indicated. Notation is the same as in Fig. 6.

Pearson correlation coefficient for the DRs – $< |j_z| >$ is 0.72.

Such a dependence indicates the direct involvement of local (small-scale) electric current structures in the processes of sunspot disruption. In other words, ohmic dissipation of small-scale electric currents is one of the factors leading to the destabilization of sunspots.

It should also be noted that the higher values of local vertical electric currents in ARs with a high rate of magnetic flux decay in a sunspot may indicate sufficiently intense motions in the vicinity of the studied sunspot, such as the presence of a large number of moving magnetic elements.

Despite the fact that in some unipolar ARs with high rates of magnetic flux decay in a sunspot, the values of the average unsigned vertical current density are close to 2.5×10^{-3} A m^{-2}, no case has been recorded where the critical level of 2.7×10^{-3} A m^{-2} is exceeded (Fursyak et al., 2020a) (vertical dashed line in Fig. 6). This observation is not surprising since unipolar ARs are remnants of bipolar or multipolar regions. They have a magnetic configuration close to potential and extremely low flare activity. Consequently, the electric currents in such ARs are also weak.

2. When analyzing the relation between the magnetic flux decay rate in a sunspot and large-scale (global, distributed) electric currents in unipolar ARs (see Fig. 7 and Table 1), it was found that for sunspots with high rates of magnetic flux decay, the values of the distributed current are close to zero (within the calculated errors indicated in the seventh column of Table 1 and bars in Fig. 7). This pattern is also typical for the seven studied

sunspots with low rates of magnetic flux decay. However, in the remaining four cases, the calculated values of the distributed electric current (up to 5.0×10^{12} A), even accounting for errors, are nonzero. Considering that the distributed electric current has its own azimuthal (vortex) magnetic field, it can be assumed that such a field around a sunspot may serve as one of the stabilizing factors during its decay.

It is also worth mentioning that in all cases where a nonzero distributed electric current was detected in the analyzed ARs, its sign was positive (i.e., the electric current was directed upward, toward the observer). Thus, the direction of the large-scale electric current corresponds to the rule of current helicity distribution in hemispheres (see, for example, Abramenko, Gopasyuk, 1987; Seehafer, 1990; Pevtsov et al., 1994; Abramenko et al., 1996, and others).

5 Conclusions and discussion

We have analyzed 16 sunspots of type U and A1 according to the MMC of ARs with varying rates of magnetic flux decay in sunspots (11 ARs with low and 5 ARs with high decay rates). One of the potential factors affecting sunspot stability is the presence of electric currents. Comparing the parameters of electric currents with the magnetic flux decay rate in sunspots has revealed the following dependences:

1. The stronger the local (small-scale) electric currents near a unipolar sunspot, the faster it decays.
2. The large-scale (distributed) electric current around rapidly decaying sunspots is nearly zero and therefore does not contribute to stabilizing the sunspot decay process.
3. For four cases of slowly decaying sunspots, a nonzero distributed (global, large-scale) electric current of up to 5.0×10^{12} A has been identified. The distributed electric current direction is consistent with the rule of current helicity distribution across hemispheres. The azimuthal magnetic field induced by the presence of large-scale electric current may have a stabilizing effect on sunspot decay.

Thus, small-scale electric currents tend to have a destabilizing effect on a sunspot, while the large-scale electric current with its own magnetic field is able to contribute to sunspot stabilization. However, it is evident that electric currents are not the only mechanism in sunspot stabilization/destabilization processes, and further research in this direction is required.

Furthermore, it should be noted that our analysis was based on a relatively small sample of ARs of type U (unipolar) and A1 (late-stage bipolar ARs with well-developed leading spots and pores in the trailing part of the AR), which represents extreme cases in terms of the magnetic flux decay rate in sunspots for the most effective detection of expected effects. The magnetic flux criterion according to which we only analyze ARs with a magnetic flux imbalance of above 50% was not applied here. However, if this criterion is included in the rules used to select ARs for analysis, the number of the studied ARs can be reduced to 12, but the correlation in Fig. 6 can decrease slightly (from 0.72 at N = 16 to 0.70 at N = 12).

Acknowledgments. The authors are grateful to the referee for interest in the work and valuable comments. This work was supported by the Ministry of Science and Higher Education of the Russian Federation (state assignment No. 122022400224-7).

References

Abramenko V.I., Gopasyuk S.I., 1987. Izv. Krymsk. Astrofiz. Observ., vol. 76. pp. 147–168. (In Russ.)
Abramenko V.I., Wang T., Yurchishin V.B., 1996. Solar Phys., vol. 168, pp. 75–89.
Abramenko V.I., Zhukova A.V., Kutsenko A.S., 2018. Geomagnetism and Aeronomy, vol. 58, iss. 8, pp. 1159–1169.
Cowling T.G., 1946. Mon. Not. Roy. Astron. Soc., vol. 106, pp. 218–224.
Fursyak Yu.A., 2018. Geomagnetism and Aeronomy, vol. 58, no. 8, pp. 1129–1135.
Fursyak Yu.A., Abramenko V.I., Kutsenko A.S., 2020. Astrophysics, vol. 63, no. 2, pp. 260–273.
Fursyak Yu.A., Kutsenko A.S., Abramenko V.I., 2020. Solar Phys., vol. 295, p. 19.
Goode P.R., Denker C.J., Didkovsky L.I., Kuhn J.R., Wang H., 2003. Journal of the Korean Astronomical Society, vol. 36, S1, pp. S125–S133.
Harvey K., Harvey J., 1973. Solar Phys., vol. 28, pp. 61–71.
Hoeksema J.T., Liu Y., Hayashi K., Sun X., Schou J., et al., 2014. Solar Phys., vol. 289, pp. 3483–3530.
Ivanov S.D., Maksimov V.P., 1978. Soviet Astronomy Letters, vol. 4, pp. 127–128.
Kosugi T., Matsuzaki K., Sakao T., Shimizu T., Sone Y., et al., 2007.·Solar Phys., vol. 243, pp. 3–17.
Krivodubskii V.N., 1983. Byulletin Solnechnye Dannye Akademie Nauk USSR, no. 11, pp. 51–57.
Kubo M., Shimizu T., 2007. Astrophys. J., vol. 671, pp. 990–1004.
Kubo M., Lites B.W., Shimizu T., Ichimoto K., 2008. Astrophys. J., vol. 686, pp. 1447–1453.
Litvinenko Yu.E., Wheatland M.S., 2015. Astrophys. J., vol. 800, p. 130.
Martinez Pillet V., 2002. Astron. Nachr., vol. 323, no. 3/4, pp. 342–348.
Meyer F., Schmidt H.U., Weiss N.O., Wilson P.R., 1974. Mon. Not. Roy. Astron. Soc., vol. 169, pp. 35–57.
Muller R., Mena B., 1987. Solar Phys., vol. 112. pp. 295–303.
Nye A., Bruning D., Labonte B.J., 1988. Solar Phys., vol. 115, pp. 251–268.
Pesnell W.D., Thompson B.J., Chamberlin P.C., 2012. Solar Phys., vol. 275, pp. 3–15.
Pevtsov A.A., Canfield R.C., Metcalf T.R., 1994. Astrophys. J., vol. 425, p. L117.
Plotnikov A.A., Kutsenko A.S., 2021. 16th Annual Conference on Plasma Physics in the Solar System. Collection of abstracts, p. 25. (In Russ.)
Scherrer P.H., Schou J., Bush R.I., Kosovichev A.G., Bogart R.S., et al., 2012. Solar Phys., vol. 275, pp. 207–227.
Seehafer N., 1990. Solar Phys., vol. 125, pp. 219–232.

Sheeley N.R., Bhatnagar A., 1971. Solar Phys., vol. 19, pp. 338–346.
Solov'ev A.A., 1976. Byulletin Solnechnye Dannye Akademie Nauk USSR, no. 7, pp. 73–78.
Solov'ev A.A., 1976. Sov. Astron., vol. 20, pp. 75–78.
Solov'ev A.A., 1984. Byulletin Solnechnye Dannye Akademie Nauk USSR, no. 1, pp. 73–78.
Solov'ev A.A., 1991. Sov. Astron., vol. 35, pp. 83–86.
Solov'ev A.A., Kirichek E., 2014. Astrophys. Space Sci., vol. 352, pp. 23–42.
Strecker H., Schmidt W., Schlichenmaier R., Rempel M., 2021. Astron. Astrophys, vol. 649, p. 123.
Zeleniy L.M., Milovanov A.V., 1993. Sov. Astron. Lett., vol. 18, pp. 249–251.
Zhukova A.V., 2018. Izv. Krymsk. Astrofiz. Observ., vol. 114. no. 2. pp. 74–86. (In Russ.)